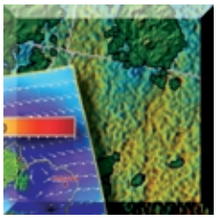

SAR Signatures of the Marine Atmospheric Boundary Layer: Implications for Numerical Forecasting

George S. Young

Synthetic aperture radar (SAR) offers the potential for 10 to 100 times higher-resolution remote sensing of the wind field at sea than is possible with spaceborne scatterometers. With this enhanced resolution comes new opportunities for quantitative analysis of marine atmospheric boundary layer (MABL) processes. In particular, SAR's ability to resolve much of the turbulence spectrum permits quantitative diagnosis of air–sea fluxes as well as the depth and stability of the MABL. Because the cost of a SAR satellite is closely linked to its resolution, it is essential to examine the minimum resolution required for each of these capabilities. The well-known similarity forms of the MABL's wind speed spectrum provide the basis for this evaluation. (Keywords: Air–sea fluxes, Atmospheric boundary layer, Similarity theory, Turbulence spectrum.)

INTRODUCTION

Synthetic aperture radar (SAR) senses that part of the sea surface roughness spectrum with wavelengths suitable for backscattering the radar beam. These relatively short gravity-capillary waves can be forced and modulated by both oceanographic and atmospheric phenomena. Thus, any oceanographic or atmospheric phenomenon capable of forcing or modulating the short-wavelength part of the sea wave spectrum can, in theory, be monitored by SAR.[1] In practice, SAR-based monitoring of oceanographic and atmospheric phenomena is both rewarding and challenging because of the very diversity of phenomena active in this process. The superposition of oceanographic phenomena (e.g., sea wave modulation by current shears) with meteorological phenomena (e.g., patchy forcing of sea waves by convective eddies) makes quantitative analysis of SAR images particularly difficult. Nonetheless, useful atmospheric data can often be obtained from SAR imagery by careful, quantitative processing.[2–5]

Wind speed information is the easiest to obtain because the atmospheric signatures in SAR imagery result from wind-driven stress roughening of the sea surface. Since the SAR wavelengths in use correspond to sea waves with relatively short lifetimes, meteorological phenomena with scales of 100 m and a few minutes can be resolved. Thus, the sea surface roughness pattern observed by SAR can capture an image of the wind speed field across much of the spectrum of atmospheric phenomena. Scatterometry[6] has long used this capability on the synoptic (resolution >2000 km), meso-alpha

(resolution 200–2000 km), and meso-beta (resolution 20–200 km) scales. SAR's much higher horizontal resolution (20–200 m) allows one to examine the patterns in the meso-gamma (2–20 km), micro-alpha (200–2000 m) and micro-beta (20–200 m) scales. The micro-alpha range is the energy-containing part of the marine atmospheric boundary layer (MABL) turbulence spectrum,[7] whereas the micro-beta range is the upper end of the inertial subrange part the spectrum. The meso-gamma range includes the spectral gap between turbulence and weather as well as most convective storms.[8,9] SAR's enhanced resolution compared with spaceborne scatterometry therefore opens up for quantitative examination several important classes of atmospheric phenomena. Given sufficiently quantitative SAR backscatter imagery and a verified quantitative theory for these phenomena, their forcing and scaling parameters can, in theory, be deduced from their SAR signatures. These quantities include boundary-layer depth and the surface fluxes of buoyancy and momentum. Thus, they are of great interest in climate analysis, weather analysis, and the initialization and verification of numerical weather prediction models.

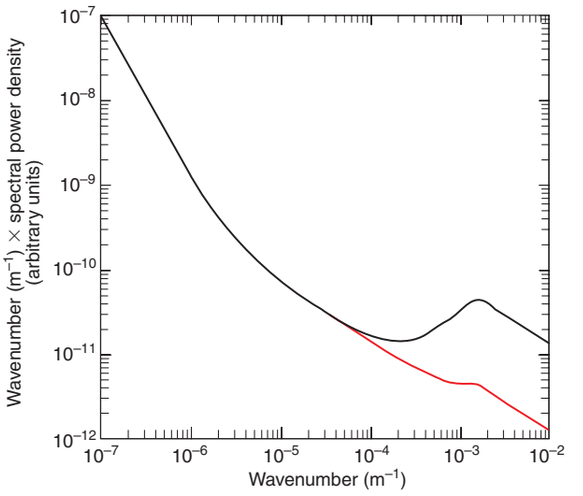

Figure 1. Schematic of the spectral subranges (black curve) of the Earth's boundary layer wind field. The plot extends from a 10,000-km wavelength at the left to 100 m at the right. From 10,000 km down to about 500 km, a −3 power law holds. From there down to about 10 km, a −5/3 power law holds. At yet smaller scales, a +1 power law, then the microscale peak, and finally another −5/3 power law holds. Note that the microscale peak may be absent if forcing for three-dimensional turbulence is weak. The spectrum for a hypothetical, very intense, but somewhat shallow boundary layer is depicted here. The red curve, which diverges as shown, represents the same as the black, but with a much weaker microscale production of three-dimensional turbulence.

ATMOSPHERIC DYNAMICS

Spectral Subranges

The atmospheric wind speed spectrum at the sea surface includes the effects of energy sources at the synoptic scale, mesoscale, and microscale. The primary synoptic-scale energy source is baroclinic instability, manifested as amplifying Rossby waves.[10] On the mesoscale, a number of energy-producing solenoidal circulations exist, ranging from thunderstorms to sea-breeze–type circulations associated with sea surface temperature boundaries. Two energy sources dominate on the microscale—shear production of turbulence and buoyant production. In all three spectral ranges, energy production is concentrated in a relatively narrow band of scales, i.e., the energy-producing subranges. Between these energy-producing subranges, the wind speed spectrum is determined by interscale cascades of energy and enstrophy (vorticity variance). These features are depicted on the schematic wind spectrum in Fig. 1.

The upper subranges of the mesoscale, including the meso-alpha and often meso-beta scales, are generally dominated by such cascades.[10] In the meso-alpha, the spectral slope is generally −3 as a result of a downscale enstrophy cascade in geostrophic two-dimensional turbulence. In the meso-beta, the −5/3 spectral slope reflects an upscale energy cascade in quasi–two-dimensional turbulence. Lilly[10] points out that these cascades can indeed overlap without affecting the spectra. Thus, the enstrophy cascade continues down into the meso-beta and the energy cascade up into the meso-alpha, despite the change in spectral slope that occurs between these two spectral subranges.

Depending on the occurrence of thunderstorms or surface-driven solenoidal circulations, the meso-gamma subrange of the wind speed spectrum may reflect the tail of this mesoscale cascade (if no energy sources are operating in that spectral range), or may have a spectral peak (if mesoscale energy sources are abundant). Thus, the meso-gamma subrange of the wind speed spectrum is highly variable, depending on the synoptic setting and nearby topographic and oceanographic features.[8]

If either of the turbulent energy production sources are active, a peak in the wind speed spectrum will be created in the microscale. Buoyant production generally results in a peak in the larger-wavelength end of the micro-alpha scale, whereas shear production is more likely to contribute in the smaller-wavelength end of the micro-alpha scale or in the micro-beta scale.[11] At scales below these energy-producing subranges, an inertial cascade of energy dominates. This cascade from large to small scales ends in viscous dissipation on the Kolmogorov microscale.[12] The dynamics of this inertial energy cascade dictate a −5/3 power law relation between the spectral density and inverse wavelength in this subrange.

Similarity Theories

The Buckingham Pi theorem has been used to derive fluid dynamics similarity theories for each of the microscale subranges of wind speed spectrum.[11] When shear production of turbulence dominates over buoyant production, Monin–Obukhov surface-layer similarity results.[11] This theory collapses the spectra of *in situ* observations onto a family of curves. Which curve a given observed spectrum fits depends solely on the height at which it was taken, normalized by the Obukhov length. The scaling parameters in Monin–Obukhov similarity are the surface momentum flux, the surface buoyancy flux, and the ratio of gravitational acceleration to the surface virtual potential temperature. All of the curves in this family exhibit a peak in the energy-producing subrange and a $-5/3$ dependence in the inertial subrange. Although well-tested via *in situ* observations, this class of wind speed spectra has yet to be clearly separated from oceanographic "clutter" in SAR imagery.

When, in contrast, buoyant production of turbulence dominates over shear production, mixed-layer similarity theory is more appropriate for surface-layer wind speed spectra.[13,14] This theory collapses the wind speed spectrum onto curves that vary with the relative orientation of the wind direction and the sampling direction. The scaling parameters responsible for this collapse are boundary-layer depth, surface buoyancy flux, and the ratio of gravitational acceleration to the surface virtual potential temperature. Along-wind spectra tend to exhibit shear distortion of the peak associated with energy production. At smaller scales, many decades of inertial subrange are generally present. SAR pixels are small enough to resolve both the spectral peak and at least a decade of the inertial subrange in these buoyantly driven MABLs, as shown schematically by the black curve in Fig. 1. The microscale peak associated with the buoyant production of turbulence is readily apparent whenever the buoyant production is sufficiently strong relative to the inertial cascade of energy down from larger (meso and synoptic) scales. Thus, the peak is present in low-wind, high-instability cases but absent or nearly so in high-wind, near-neutral cases as shown schematically by the red curve in Fig. 1.

The wavelength of the microscale peak in the wind speed spectrum of a convective boundary layer is proportional to the only other length scale available in mixed-layer similarity, the boundary-layer depth Z_i. The wavelength of the spectral peak is generally observed to be 1.5 times the boundary-layer depth.[2,11] Thus, the spectral analysis of SAR imagery and the application of this ratio to the wavelength of the resulting micro-scale spectral peak can be used to infer the MABL depth from space.[2] The method, being based on mixed-layer similarity theory, is only valid for unstable boundary layers and so fails when boundary-layer convection is weak or the surface wind speed is strong. Under favorable conditions, the results can be accurate to within better than 20%.[2] A map of boundary-layer depth may be obtained by spectrally analyzing subimages. The minimum subimage for accurate estimates of boundary-layer depth is a square with sides approximately $10\,Z_i$ long. In practice, this works out to sides of 5 to 10 km.

Because the amplitude of the surface wind speed spectrum in unstable conditions obeys mixed-layer similarity theory, one can invert the similarity formulas to obtain the surface fluxes of momentum and buoyancy.[3,4] In theory, a similar approach using Monin–Obukhov similarity could be applied in stable boundary layers to obtain these same quantities. Such an analysis has not yet been undertaken since wind speeds in sufficiently stable conditions are often below SAR detection limits.

Because separate mixed-layer similarity theories exist for the inertial subrange and for the integrated area under the spectrum (wind speed variance), there are two possible algorithms for backing the surface fluxes out of the SAR spectra of unstable MABLs.[3,4] The first approach inverts the relationship between the gust ratio (wind speed divided into its standard deviation) and the relative intensities of shear and buoyant production of turbulence. The latter ratio is quantified by the ratio of the boundary-layer depth to the Obukhov length. Because the boundary-layer depth can be determined from SAR imagery as described previously, the only unknown is the Obukhov length. Once it has been solved for, it can, in theory, be used to relate the SAR-measured surface momentum flux (stress) to the true wind speed using Monin–Obukhov wind profile relations.[15] Likewise, the mathematical definition of the Obukhov length and the SAR-measured surface momentum flux can be used to calculate the surface buoyancy flux. The SAR-derived boundary-layer depth and surface buoyancy flux provide sufficient information to calculate the convective-scale velocity[11] as well. Sensitivity studies of this analysis technique[4] reveal that the stability correction to wind speed is not particularly sensitive to uncertainty in the SAR input, whereas the derived buoyancy flux is quite sensitive. Owing to a fortuitous cube root in its definition,[11] the convective-scale velocity is also relatively insensitive to uncertainty in the SAR input.

These same quantities can be inferred using the mixed-layer similarity theory for the wavelength-dependent power in the inertial subrange of the convective MABL's wind speed spectrum.[4] Given the SAR-determined boundary-layer depth, the only unknown in this similarity theory is the convective-scale velocity. Thus, the convective-scale velocity can, in theory, be determined by fitting the theoretical curve

to the inertial subrange of the SAR-observed wind speed spectrum. The surface buoyancy flux is then backed out of the formal definition of the convective-scale velocity. The number of poorly known constants in this theory limits the formal sensitivity analysis of its results. However, the large number of observations in a SAR image compared with the usual atmospheric time series offers the opportunity to deduce the values of these constants much more robustly than is possible with *in situ* measurements. Preliminary investigation of this possibility suggests that the most broadly accepted values for the spectral constants are probably more accurate than previously supposed and that the scatter in previously reported values is due more to undersampling by *in situ* sensors than to natural variation in these constants.

SAR OBSERVATIONS

SAR observations of surface wind speed spectra reflect the theoretical results already discussed. In situations such as that captured in Fig. 2a, when the buoyant production of turbulence dominates the inertial cascade from larger scales, a clear microscale peak such as that in Fig. 2b occurs. This dominance of buoyant production requires an unstable stratification at the air–sea interface. It does not necessarily require low wind speeds, although the instability requirements decrease with decreasing wind speed. Essentially, the existence of a microscale peak depends on the convectively driven gusts standing out above the wind-driven microscale tail of the mesoscale spectrum. If this occurs, the peak at a wavelength of 1.5 Z_i and a spectral gap at a wavelength of roughly 10 Z_i are observed. As the relative contribution of the wind-driven turbulence increases (e.g., Fig. 3a), the gap fills from the long wavelength end and so moves to shorter wavelengths (Fig. 3b), until, for high enough wind speeds, it obliterates the peak.

At low wind speeds, the SAR-observed inertial subrange also matches theoretical expectations, as seen in Fig. 2b. At higher wind speeds, however, the white noise floor increases, gradually wiping out the weaker short-wavelength end of the inertial subrange. This white noise shows up on the SAR imagery as speckle, perhaps related to breaking waves or other stochastic effects of wave–wave interaction. At high wind speeds, the sea surface speckle spectrum dominates that of the atmospheric turbulence, and meteorological analysis becomes impossible.

In situ verification of SAR-derived wind speeds is complicated by the turbulent nature of the true wind speed field. Because the power in the observed wind speed spectrum is spread over a broad wavelength band, an instantaneous point measurement is unlikely to be representative of the pixel in which it was collected, regardless of the pixel's size. To obtain meaningful comparison of such a broad spectrum signal, one must average the *in situ* wind speed observations over scales corresponding as exactly as possible to the SAR image area used to provide the wind speed estimate being

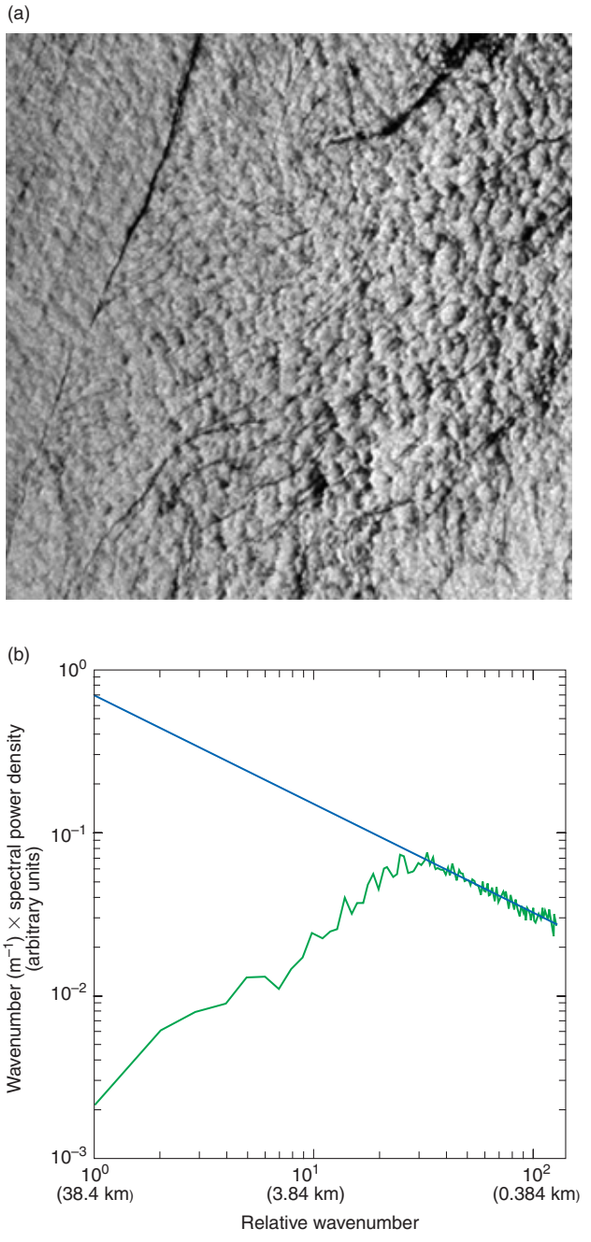

Figure 2. A 256 × 256 pixel European Remote Sensing satellite (ERS-1) SAR image of the Gulf Stream taken at 1538 UT on 17 June 1993 (a), and the resulting power spectra (b). Pixel size is 150 m, so wavenumber 1 corresponds to a wavelength of 38,400 m. The microscale peak at a wavelength of about 1 km occupies the central wavenumbers, while its −5/3 slope inertial subrange tail dominates the high wavenumbers. The straight line plotted for comparison has a −5/3 spectral slope, −2/3 on this wavenumber-scaled plot. The low wavenumber tail of the microscale peak extends out to the longest wavelengths sampled.

verified. Such comparison of time averages with space averages is problematical at best, because the broadband nature of the wind speed spectrum requires that observations be collocated in space and time before agreement can be expected. These statistical problems become increasingly severe as the SAR area used to produce a single wind speed estimate decreases, because the percent of the true wind variance averaged away decreases as the averaging area decreases. Thus, it is not surprising that *in situ* verification studies often show poor correlations for small analysis areas.

In situ verification of SAR-derived wind speed spectra, rather than wind speed itself, may ease the task somewhat, but only at the price of losing phase information. Much more thought and careful experimentation are needed before making definite statements about the lower scale limits of SAR wind speed retrieval. At present, one can only state that some SAR wind speed spectra match atmospheric theory down to pixel sizes of 150 m.

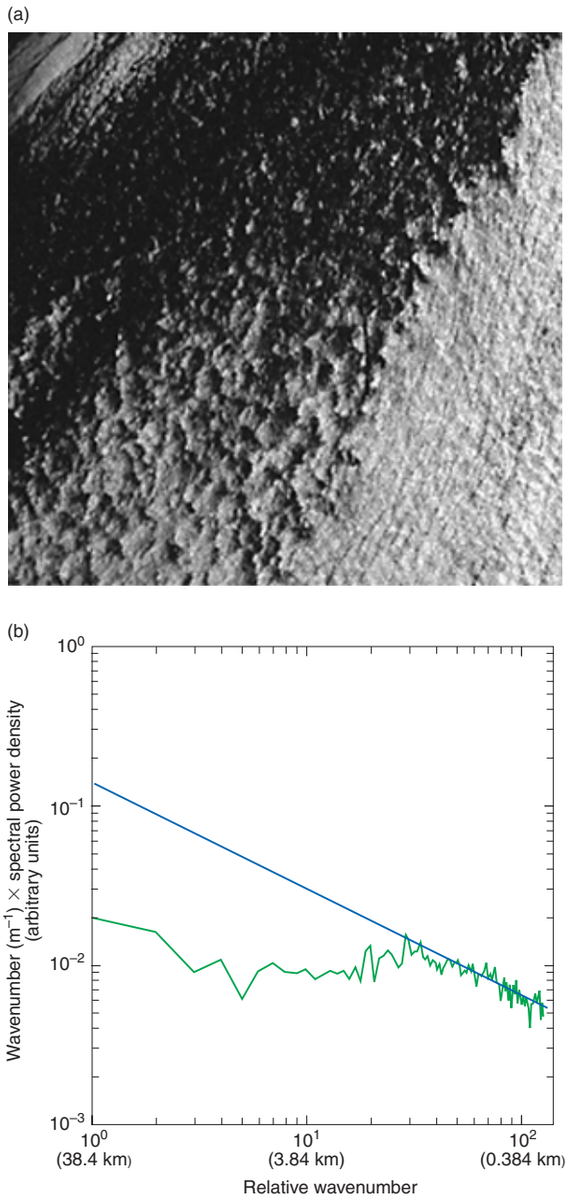

Figure 3. Same as Fig. 2 for a second SAR image. Here, the tail of the mesoscale is seen at low wavenumbers. The microscale peak is still distinguishable, as is the inertial subrange.

SAR IMPLICATIONS

Resolution Requirement

Each of the quantitative analysis methods presented in the previous discussion imposes resolution constraints on the SAR imagery. For deducing the boundary-layer depth, the SAR pixel size must be roughly a factor of 6 smaller than Z_i (i.e., a factor of 9 smaller than the microscale spectral peak). Thus, over tropical seas where Z_i is typically around 600 m, the pixel size should be 100 m or smaller if boundary-layer depth is to be monitored. In the subtropics, the boundary-layer depth is more variable and the required pixel size could be as small as 50 m. Similar resolution should suffice for finding fluxes via the SAR-measured microscale wind speed variance, provided care is taken to use mixed-layer spectral similarity to account for the unsampled variance at subpixel scales. The alternative approach to finding the surface fluxes using inertial subrange similarity theory requires somewhat finer resolution, since the pixel size should be at least a decade down into the inertial subrange scales. Thus, pixel sizes of 10 to 50 m may be needed, depending on the boundary-layer depth.

In any case, it is pointless from the meteorological perspective to reduce pixel size below that for which wind retrieval is possible, that is, below the area of wind effectively averaged by the time required for the surface stress to bring the SAR-relevant portion of the wave spectrum into balance with a local wind fluctuation. This issue lies in the realm of gravity-capillary wave dynamics. For most conditions, Taylor's frozen turbulence hypothesis holds, so the wind speed can be used to convert the time required for the SAR-relevant waves to reach equilibrium into a minimum pixel size for wind speed retrieval.

Physical Constraints

The quantitative analysis techniques outlined in this article will also fail whenever the air–sea interface doesn't provide adequate atmospheric signatures. For example, if the MABL turbulence is weak relative to the short-wavelength tail of the mesoscale spectrum, there will be no microscale peak or inertial subrange

to analyze. This condition can be caused by either near-neutral stratification (i.e., via a weak turbulence contribution to the spectrum) or high wind speeds (i.e., via a strong mesoscale contribution to the spectrum). Inertial subrange information is also lost at high wind speeds, since breaking seas lead to stochastic speckle and the spectrum becomes dominated by white noise. In contrast, under stable conditions, the wind speed and surface stress frequently fall below SAR detection limits. The threshold wind speed at which these other effects mask the turbulence contribution to the spectrum depends on the intensity of the turbulence itself.

The contamination of SAR imagery due to oceanographic phenomena is a major complication in the analysis methods outlined here. Some oceanographic signatures can be eliminated by proper filtering in spectral space, particularly if atmospheric similarity theory is used to reconstruct the damaged portions of the spectrum. Often, however, strong oceanographic features swamp key spectral subranges, precluding quantitative meteorological analysis. While posing a problem for meteorologists, these conditions provide a ray of hope for oceanographers, bringing the phenomena of interest to them above the "meteorological noise floor." Much of the time one or the other set of phenomena dominates sufficiently to please at least one of these communities.

CONCLUSIONS

The foregoing discussion provides quantitative insight into the resolution dependence of a SAR's utility for quantitative analysis of the MABL. If wind speed retrieval proves possible down to those scales, a pixel size of 100 m will frequently suffice to obtain estimates of the MABL turbulence intensity, MABL depth, the convective-scale velocity, and the surface buoyancy flux. Reducing the pixel size to 50 m allows a second semi-independent means of estimating these parameters. Both of these methods will provide more accurate estimates as the pixel size is decreased, again subject to the eventual breakdown of wind speed retrieval. Both will fail in near-neutral, high-wind, or stable MABLs, no matter what pixel size is used.

Going to pixel sizes greater than 100 m greatly limits the regions of the Earth over which quantitative analyses can be made of these meteorological parameters. As resolution degrades, the analysis is limited to progressively deeper (and thus rarer) boundary layers. For example, a SAR with 300-m pixels may sometimes resolve enough of the wind speed spectrum to allow estimation of Z_i but rarely enough to permit estimation of the surface buoyancy flux or other turbulence statistics. In the limit, a SAR with 1-km or larger pixels cannot be used with existing similarity theories to derive quantitative estimates of any MABL parameters except wind speed and direction. Those would have to be derived via spaceborne scatterometry.

REFERENCES

[1] Vesecky, J. F., and Stuart, R. H., "The Observation of Ocean Surface Phenomena Using Imagery from SEASAT Synthetic Aperture Radar: An Assessment," *J. Geophys. Res.* **87**, 3397–3430 (1982).

[2] Sikora, T. D., Young, G. S., Shirer, H. N., and Chapman, R. D., "Estimating Convective Atmospheric Boundary Layer Depth from Microwave Radar Imagery of the Sea Surface," *J. Appl. Meteorol.* **36**, 833–845 (1997).

[3] Young, G. S., Sikora, T. D., and Thompson, D. R., "A Method for Relating SAR Backscatter from the Sea Surface to Atmospheric Boundary Layer Turbulence Statistics," in *4th Thematic Conf. on Remote Sensing for Marine and Coastal Environments*, ERIM, Vol. II, pp. 201–210 (Mar 1997).

[4] Young, G. S., Sikora, T. D., and Thompson, D. R., "Stability Correction of Surface Winds Derived from Synthetic Aperture Radar," in *Proc. 12th Symp. on Boundary Layers and Turbulence*, American Meteorological Society, pp. 486–487 (Jul 1997).

[5] Young, G. S., and Sikora, T. D., "Distinguishing Boundary Layer Signatures from Mesoscale and Ocean-Clutter in SAR Imagery," in *Proc. IEEE Int. Geoscience and Remote Sensing Symp.*, Seattle, WA (Jul 1998).

[6] Stoffelen, A. C. M., and Anderson, D. L. T., "ERS-1 Scatterometer Characteristics and Wind Retrieval Skill," in *Proc. 1st ERS-1 Symp.*, ESA-0SP 359, Vol. 1, pp. 41–47 (1993).

[7] Young, G. S., "Mixed Layer Spectra from Aircraft Measurements," *J. Atmos. Sci.* **44**, 1251–1256 (1987).

[8] Nicholls, S., and LeMone, M. A., "The Fair Weather Boundary Layer in GATE: The Relationship of Subcloud Fluxes and Structure to the Distribution and Enhancement of Cumulus Clouds," *J. Atmos. Sci.* **37**, 2051–2067 (1980).

[9] Nucciarone, J. J., and Young, G. S., "Aircraft Measurements of Turbulence Spectra and the Marine Stratocumulus-Topped Boundary Layer," *J. Atmos. Sci.* **48**, 2382–2392 (1991).

[10] Lilly, D. K., "Two-Dimensional Turbulence Generated by Energy Sources at Two Scales," *J. Atmos. Sci.* **46**, 2026–2030 (1989).

[11] Kaimal, J. C., Wyngaard, J. C., Haugen, D. A., Cote, O. R., and Izumi, Y., "Turbulence Structure of the Convective Boundary Layer," *J. Atmos. Sci.* **33**, 2152–2169 (1976).

[12] Tennekes, H., and Lumley, J. L., *A First Course in Turbulence*, MIT Press, Cambridge, MA (1972).

[13] Panofsky, H. A., Tennekes, H., Lenschow, D. H., and Wyngaard, J. C., "The Characteristics of Turbulent Velocity Components in the Surface Layer Under Convective Conditions," *Boundary Layer Meteorol.* **11**, 355–361 (1977).

[14] Panofsky, H. A., and Dutton, J. A., *Atmospheric Turbulence*, Wiley-Interscience, New York (1984).

[15] Fairall, C. W., Bradley, E. F., Rogers, D. P., Edson, J. B., and Young, G. S., "Bulk Parameterization of Air-Sea Fluxes for TOGA COARE," *J. Geophys. Res.* **101**, 3734–3764 (1996).

ACKNOWLEDGMENTS: Preparation of this material was funded by the National Science Foundation through grant ATM-9629567. Special thanks to Drs. Tom Georges and Jack Harlan for insightful discussions on the relationship between the wavelength and equilibrium timescales of ocean waves.

THE AUTHOR

GEORGE S. YOUNG is with the Department of Meteorology, The Pennsylvania State University. His e-mail address is young@ems.psu.edu.